Analysis and Correction of Gradient Nonlinearity and B_0 Inhomogeneity Related Scaling Errors in Two-Dimensional Phase Contrast Flow Measurements

Johannes M. Peeters,[1*] Clemens Bos,[2] and Chris J. G. Bakker[1]

Phase contrast flow measurements will be increasingly biased at eccentric positions, where nonlinearity of gradients and inhomogeneity of the main field become important. In theory, they scale the result of phase contrast flow values in two ways: incorrect velocity encoding of moving spins and geometric distortion of the vessel cross-sectional area. A flow phantom, consisting of a 3D grid of interconnected tubes, was used to determine the spatial dependence of the associated scaling factors, which demonstrate that scaling errors in flow can be as large as 20% within the examined volume of 336 × 336 × 336 mm^3. The same phantom was also used to determine and minimize concomitant gradient effects. Correction of the off-center flow values with the local scaling factors and the concomitant gradient phase improves the measurement accuracy substantially, both in the flow phantom and in a volunteer study. Magn Reson Med 53:126–133, 2005. © 2004 Wiley-Liss, Inc.

Key words: phase contrast imaging; flow quantification; gradient nonlinearity; image distortion; hemodialysis

In the past decade, numerous studies have been devoted to the sources of errors in phase contrast (PC) flow quantification (1–8). Factors affecting the accuracy and precision of these measurements have been investigated extensively and include aliasing due to mismatched encoding velocity, intravoxel phase dispersion, angulation of the imaging plane, inadequate temporal and/or spatial resolution, pulsatility effects, phase offset errors, measurement noise, and spatial misregistration. As far as we know, only one study includes off-center velocity miscalculation related to gradient nonuniformity (9). Our interest in off-center miscalculation of flow was aroused by some inconsistent results of a study in which flow measurements were performed in the loop graft in the forearm of hemodialysis patients (Fig. 1). On average, PC measurements in these grafts were 9% higher than ultrasound dilution measurements (10) and, occasionally, significant differences were observed between the flow values of the arterial and venous limbs. We hypothesized that these observations could have been caused by the nonlinearity of gradients and the inhomogeneity of the main field, as they increase further off-center. Therefore, we performed a theoretical and experimental analysis of the influence of measurement position on PC flow measurements. In the theoretical part, we will show that scaling of the reconstructed vessel cross-sectional area, caused by inhomogeneity of the main field and nonlinearity of the read and phase-encoding gradients, and scaling of the reconstructed velocity, caused by the nonlinearity of the velocity-encoding gradient, result in incorrect flow values. In the experimental section, we will demonstrate that the associated scaling factors can be determined with a flow phantom and that they can be used to correct the observed flow values. Furthermore, we will show that at off-center positions, concomitant gradients will degrade PC flow measurements. We use the same flow phantom to measure and minimize the sequence-dependent concomitant phase evolution in order to quantify this effect. We will demonstrate concomitant gradient correction in combination with scaling correction, both in the flow phantom and in a volunteer study.

THEORY

The volume flow Q through a vessel is the integral of the velocity profile over the cross-sectional area of the vessel. With PC techniques, it is possible to measure velocity, which enables flow quantification by adding the velocity contents over the cross-sectional area. However, the reconstructed cross-sectional area and velocity will be scaled due to the nonlinearity of gradients and inhomogeneity of the main field, resulting in incorrect 2D PC flow values.

Inhomogeneity of the Main Field

Reichenbach et al. (11) explain distortions of the image in gradient echo imaging as a result of inhomogeneity of the main field, resulting in scaling, translation, and shearing of the object in the read direction. Scaling arises from local, stationary gradients in the read direction, shearing from local, stationary gradients in the phase direction, and translation from a local field offset. We will take a closer look at scaling as it influences the size of the reconstructed cross-sectional area. The local, stationary gradient $G'_{\Delta B}(\mathbf{r})$ in the read direction x, resulting from the spatial field inhomogeneity $\Delta B_0(\mathbf{r})$, can be approximated by

$$G'_{\Delta B}(\mathbf{r}) = \frac{\Delta B_0(\mathbf{r} + \Delta\mathbf{r}) - \Delta B_0(\mathbf{r})}{\Delta\mathbf{r}} = \frac{\Delta B_0(x + \Delta x, y, z) - \Delta B_0(x, y, z)}{\Delta x}. \quad [1]$$

[1]Image Sciences Institute, Department of Radiology, University Medical Center Utrecht, Utrecht, The Netherlands.

[2]Laboratoire d'Imagerie Moleculaire et Fonctionelle, ERT CNRS, Université 'Victor Segalen' Bordeaux 2, Bordeaux, France.

Part of this work was presented at the 12th Annual Meeting of the International Society for Magnetic Resonance in Medicine, Kyoto, Japan, 2004.

Grant sponsor: Dutch Technology Foundation STW; Grant number: UPG 5441.

*Correspondence to: Hans Peeters, Image Sciences Institute, UMC, Room E01.335, Heidelberglaan 100, 3584 CX Utrecht, The Netherlands. E-mail: hans@isi.uu.nl

Received 13 February 2004; revised 9 August 2004; accepted 11 August 2004.

DOI 10.1002/mrm.20309
Published online in Wiley InterScience (www.interscience.wiley.com).

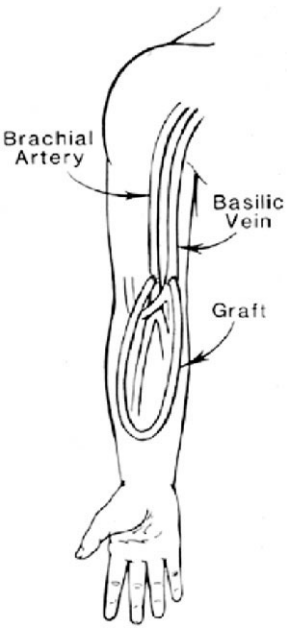

FIG. 1. Drawing of the forearm of a hemodialysis patient with a loop graft.

The actual local read gradient during sampling is not G_x, but has been changed to $G_x + G'_{\Delta B}$ and thereby scales the object by a factor $\lambda_{\Delta B}^{-1}$, with

$$\lambda_{\Delta B}(\mathbf{r}) = \frac{G_x}{G_x + G'_{\Delta B}(\mathbf{r})}. \quad [2]$$

If $\lambda_{\Delta B} > 1$, the object will appear shrunken; if $\lambda_{\Delta B} < 1$, the object will appear stretched. The stationary gradient $G'_{\Delta B}$ also causes an echo shift in time, resulting in signal loss and a lower signal-to-noise ratio (SNR). The random phase error, and with that the random error in reconstructed velocity, will increase (8,12), leading to a lower precision of the flow measurement.

Nonlinearity of the In-Plane Gradients

Nonlinearity of the in-plane gradients causes scaling of the object similar to a local stationary gradient in the read direction. The read G_x and phase G_y gradient applied are locally scaled by a factor λ_{Gx}^{-1} and λ_{Gy}^{-1}, respectively, with $\lambda_{Gx}^{-1} = G_x(G_x+G'_x(\mathbf{r}))^{-1}$ and $\lambda_{Gy}^{-1} = G_y(G_y+G'_y(\mathbf{r}))^{-1}$. This can easily be seen by analyzing the phase evolution of the spins at a certain location (x,y) for a gradient echo sequence,

$$\begin{aligned}\phi(p,t) &= \gamma p(\Delta G_y + \Delta G'_y)y\tau_p + \gamma(G_x + G'_x + G'_{\Delta B})xt \\ &= \gamma p\lambda_{Gy}^{-1}\Delta G_y y\tau_p + \gamma(\lambda_{Gx}\lambda_{\Delta B})^{-1}G_x xt, \quad [3]\end{aligned}$$

with γ the gyromagnetic ratio, ΔG_y and p the phase gradient step and step number, τ_p the time the phase gradient is turned on, and t the readout time. The spins in a region $dxdy$ will be reconstructed in $dx_{\text{rec}}dy_{\text{rec}}$ with $dx_{\text{rec}} = (\lambda_{Gx}\lambda_{\Delta B})^{-1}dx$ and $dy_{\text{rec}} = \lambda_{Gy}^{-1}$, and the whole object is scaled by the factor $(\lambda_{Gx}\lambda_{Gy}\lambda_{\Delta B})^{-1}$. Actually, $dx_{\text{rec}} = (\lambda_{Gx}^{-1}+\lambda_{\Delta B}^{-1} - 1)dx$, but the cross term $G'_x G'_{\Delta B} G_x^{-1} \ll G_x$ and can be neglected. Equation [3] only holds if the gradient nonlinearity step $\Delta G'_y$ is proportional to the gradient step ΔG_y. Therefore, we will verify this property experimentally.

Nonlinearity of the Through-Plane Gradients

The velocity v_{rec} is determined using the phase ϕ of a pixel,

$$\phi = \gamma v_{\text{true}} M_1, \quad [4]$$

with v_{true} the velocity of the flowing spins and $M_1 = \int tG_{\text{ve}}(t)dt$ the first moment at the echo time of the velocity-encoding gradient G_{ve}. PC flow quantification techniques use bipolar gradient pulses for velocity encoding. Two acquisitions are made with opposed polarity of the bipolar gradient pulse to change the sign of the first gradient moment in order to minimize unintended phase-offset effects, e.g., caused by field inhomogeneity, eddy currents, and RF penetration effects. Phase subtraction then leads to the reconstructed velocity

$$v_{\text{rec}} = \frac{\phi_2 - \phi_1}{\gamma(M_{1,2} - M_{1,1})} = \frac{\Delta\phi}{\gamma\Delta M_1}, \quad [5]$$

where $\Delta\phi$ is the phase difference between both images and ΔM_1 the difference in first gradient moment. In the presence of a nonlinearity, the velocity-encoding gradient is locally scaled by a factor $\lambda_{G\text{ve}} = G_{\text{ve}}(G_{\text{ve}}+G'_{\text{ve}}(\mathbf{r}))^{-1}$. Thus, the first moment of G_{ve} and the reconstructed velocity will be scaled correspondingly:

$$v_{\text{rec}} = \frac{v_{\text{true}}}{\lambda_{G\text{ve}}}. \quad [6]$$

Because the bipolar velocity-encoding gradient does not need to be symmetrical between the two acquisitions, the first gradient moments ($M_{1,1}$ and $M_{1,2}$) have to be scaled in an equal way, which is the case if the gradient nonlinearity is proportional to the gradient strength. The slice selection gradient nonlinearity will influence the observed flow value in two ways. If $\lambda_{G\text{ss}} < 1$, the slice thickness decreases, resulting in a lower SNR and vice versa. The other effect is a distortion of the slice profile; the slice profile may be tilted, resulting in a scan plane not completely perpendicular to the vessel. A local gradient in the slice selection direction related to the inhomogeneity of the main field adds to the slice selection gradient nonlinearity. Neither slice thickness nor profile distortion influences the accuracy of the measured flow value much (5).

As shown above, through-plane 2D PC flow measurements depend on gradient linearity in all three orthogonal directions. In-plane gradient nonlinearity and B_0 inhomogeneity result in scaling of the cross-sectional area of the vessel, through-plane gradient nonlinearity in incorrect velocity encoding of the moving spins. For small vessels, the scaling factors λ can be assumed to be constant across the vessel cross-sectional area. Similarly, for low velocities in combination with a short echo time, $\lambda_{G\text{ve}}$ can also be

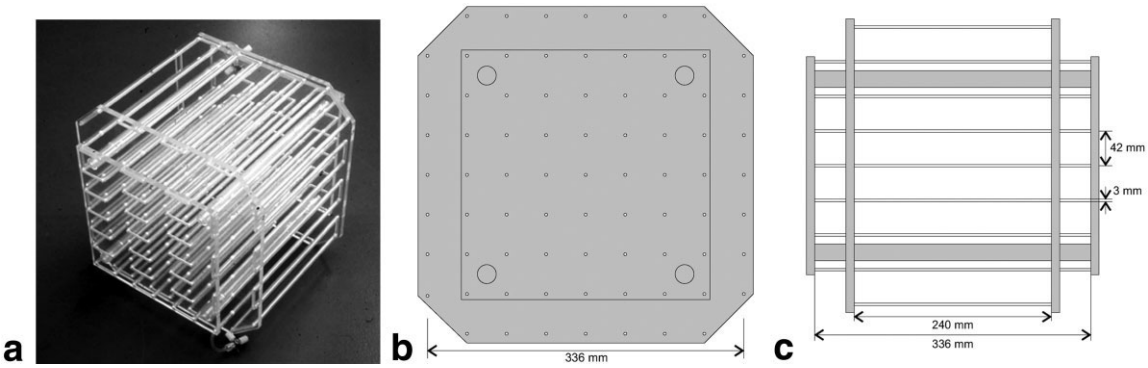

FIG. 2. The flow phantom with its dimensions: (**a**) picture, (**b**) frontal view, (**c**) lateral view.

taken into account as a constant, because the displacement of the spins will remain small. Under these assumptions, the reconstructed flow value will be inversely proportional to the product of the scaling factors:

$$\frac{Q_{\text{rec}}}{Q_{\text{true}}} = \frac{1}{\lambda_{\Delta B}\lambda_{Gx}\lambda_{Gy}\lambda_{Gve}}. \quad [7]$$

If all four scaling factors are known, correction is possible by multiplying the reconstructed flow by $\lambda_{\Delta B}\lambda_{Gx}\lambda_{Gy}\lambda_{Gve}$.

METHODS

The Flow Phantom

The experiments were performed with a flow phantom consisting of 77 serially connected, parallel tubes placed in a regular matrix (Fig. 2) (13). The phantom could be rotated in the scanner bore, such that the tubes were either parallel or perpendicular to the main field. The distance between the tubes was large enough to avoid interaction of the local fields of the tubes. The diameter of the tubes was 3 mm and was sufficiently small to assure constant scaling factors over the tube cross section. The tube at the center of the phantom was positioned at the center of the scanner bore. The circulating fluid was copper sulfate-doped water (10.0 g $CuSO_4 \cdot 4H_2O$ L water; T_1/T_2 = 32/28 msec at 1.5 T (14)), which has a low T_1 to have sufficient SNR. The tubes were surrounded by air. Steady flow was induced by a constant gravitational pressure head of 1.9 m water. Timed collection of the fluid served as a control for the 2D PC flow measurements.

Inhomogeneity Determination

First, the inhomogeneity of the main field and the gradient nonlinearity distortions were determined at the grid points of the phantom. The measured inhomogeneity and nonlinearity data were interpolated to calculate the associated scaling factors.

Machine-dependent field inhomogeneity and nonlinearity of gradients were determined using the distortion properties of a 2D FT SE sequence (15),

$$y_1 = y + \frac{\Delta B_{Gy}(\mathbf{r})}{G_y} \quad [8]$$

$$x_1 = x + \frac{\Delta B_{Gx}(\mathbf{r})}{G_x} + \frac{\Delta B_0(\mathbf{r})}{G_x}, \quad [9]$$

in which (x,y) and (x_1,y_1) refer to the true and the distorted positions, respectively. ΔB_0 is the inhomogeneity of the main field and ΔB_{Gx} and ΔB_{Gy} the gradient fields representing the nonlinearity of the read and phase gradients. Images were made with the image plane perpendicular to the tubes. The gradient nonlinearity field in the phase direction was directly calculated from subtraction of the position of a tube in image domain and its nominal position in the grid (Eq. [8]). A second image with the phase and read gradient direction exchanged allowed calculation of the gradient nonlinearity field in the other direction. The inhomogeneity of the main field was calculated by taking into account the earlier determined gradient nonlinearity field and the read gradient strength in either the first or the second image. Maps of the gradient nonlinearity in the third direction were determined after rotation of the phantom in the scanner bore by 90°.

The analysis above and, as mentioned earlier, the analyses of phase and velocity-encoding gradient scaling build on the assumption that the gradient field error is proportional to the applied gradient strength. We verified this assumption by making scans with different read gradients, in which several gradient strengths and both polarities in one direction were used. If the assumption holds, the distortion caused by ΔB_0 is inversely proportional to the read gradient strength and the positional error induced by G'_x is constant with respect to the gradient strength (Eq. [9]).

The position of the tubes in the 2D FT SE images was obtained by localizing the pixel with the maximum intensity of each tube. The center of mass was calculated around that pixel within an area of the size of the cross-sectional area of the tubes. The scaling factors of the nonlinearity of the gradients were determined by making third-order polynomial fits of the grid position as function of the distorted position in phase direction. These fits were differentiated to calculate λ_{Gy}:

$$\lambda_{Gy} = \frac{\delta y}{\delta y_1}. \quad [10]$$

λ_{Gy} is independent of the gradient strength, provided G_y and ΔB_{Gy} are proportional. However, $\lambda_{\Delta B}$ is acquisition

specific and depends on the read direction and the read gradient strength. A third-order polynomial map of $\Delta B_0(\mathbf{r})$ with respect to the read direction x was made. $\lambda_{\Delta B}$ was calculated with this map and the read gradient strength of the 2D PC acquisition according to Eqs. [1] and [2].

Concomitant Gradients

We examined the effect of concomitant gradients on PC imaging by doing some experiments with stationary fluid and different echo times, indirectly influencing the concomitant gradient phase ϕ_c; a longer TE allows more freedom in planning gradient timings and strengths. According to Bernstein et al. (16), the concomitant magnetic field B_c can, to the lowest order and for $B_0 > 0$, be described by

$$B_c(x,y,z,t) = \frac{1}{2B_0}\left\{\left(G_x z - \frac{G_z x}{2}\right)^2 + \left(G_y z - \frac{G_z y}{2}\right)^2\right\}, \quad [11]$$

which demonstrates that ϕ_c is quadratically dependent on the gradient strengths and the off-center position. When choosing a longer echo time, the gradients can be turned on longer with a lower strength, resulting in a lower ϕ_c.

Imaging

Imaging was performed on two clinical 1.5-T scanners (Gyroscan, Philips, Best, The Netherlands), which will be referred to as systems 1 and 2, respectively. To avoid frequency shifts due to wrong determination of the central frequency, the central frequency was determined with another cylinder before the phantom was placed in the magnet. This cylinder was made of PVC and filled with the same fluid as used for the 2D PC flow quantification and the 2D FT SE inhomogeneity measurements. It had a diameter of 32 mm and a length of 400 mm to simulate the infinite cylinder behavior of the tubes of the phantom and to have enough mass for central frequency determination. The orientation of the cylinder was similar to the orientation of the phantom tubes. After this procedure, the central frequency was fixed.

Transverse and sagittal multislice 2D FT SE images were acquired such that a volume of $336 \times 336 \times 336$ mm^3 was examined (9 slices with slice thickness 20 mm, slice gap 22 mm, FOV 384×384 mm^2, scan matrix 256×256, G_x = 3.4 mT/m). Low gradient strengths with low slopes were used to minimize eddy current effects.

The 2D PC flow measurements were performed in the transverse plane (slice thickness 10 mm, FOV 384×384 mm^2, TR/TE 31/20 msec, flip angle 40°, G_x = 4.5 mT/m, NEX 8). A large scan matrix of 1024×1024 was used to minimize partial volume effects (7,8). The Venc of 30 cm/sec was little above the maximum velocity in the tubes (±25 cm/sec). The pixels representing the tubes were selected in the magnitude image by thresholding at 20% of the maximum intensity, after which this mask was applied to the phase image for flow quantification. At lower threshold levels, also background pixels in the intermediate environment without signal were selected, which did not belong to the tubes.

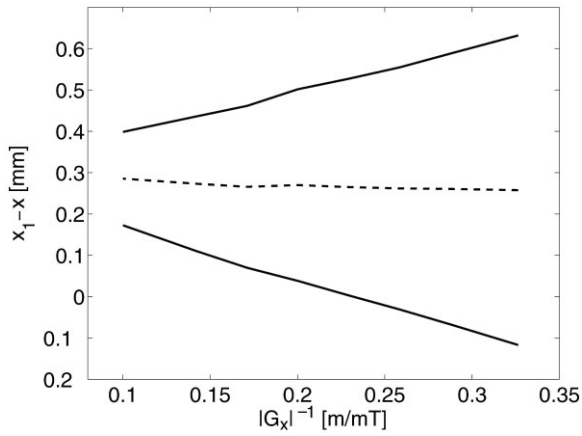

FIG. 3. Distortion for different read gradient strengths with negative and positive polarity (solid lines) and the mean of both (dashed line).

Volunteer Study

Three healthy volunteers (male, mean age 29) had a loop graft model (17) without stenosis attached to the forearm to mimic the situation in patients. Volunteer 1 was scanned with system 1 and volunteers 2 and 3 with system 2. A glycerol water mixture (T_1/T_2 = 710/140 msec) was used as the flowing fluid. PC flow measurements were performed with stationary fluid and with different steady flow rates (up to 45 mL/sec in steps of 5 mL/sec) induced by a computer-controlled pump (UDHC flow system, R.G. Shelley, Ltd., North York). The flow direction of the fluid in the model at the forearm of volunteer 2 was reversed to verify that scaling is not dependent on it. Transverse PC images were obtained with a 40×10 rectangular surface coil (slice thickness 5 mm, FOV 200×140 mm^2, scan matrix 512×360, TR/TE 16/10 msec, flip angle 10°, Venc 250 cm/sec, G_x = 6.5 mT/m, NEX 4). The rectangular surface coil was only used as receive coil to have a higher SNR. The same gradient and rf coils as in the phantom experiments were used, so the scaling parameters determined with the phantom could be applied for correction.

RESULTS

The results of the flow phantom presented here were obtained with system 1. These include the proportionality of gradient nonlinearity, the spatial dependence of B_0 inhomogeneity and gradient nonlinearity, concomitant gradient effects, and flow measurements. The results of the volunteer study were obtained with systems 1 and 2.

First, we verified the assumption that gradient nonlinearity is proportional to the gradient strength. Figure 3 shows that the distortion ($x_1 - x$) of one tube as a function of the read gradient strength and polarity can be decomposed into a part proportional to G_x^{-1} and a constant offset. The first is related to the stationary ΔB_0 and the offset to the gradient nonlinearity field (Eq. [9]), which proves that G' is proportional to G. At this point, the absolute gradient is too small, i.e., $\lambda_{Gx} > 1$.

Next, we quantified the distortion of the tubes in image domain and obtained the gradient distortion and field inhomogeneity maps. Figure 4a shows that the tubes fur-

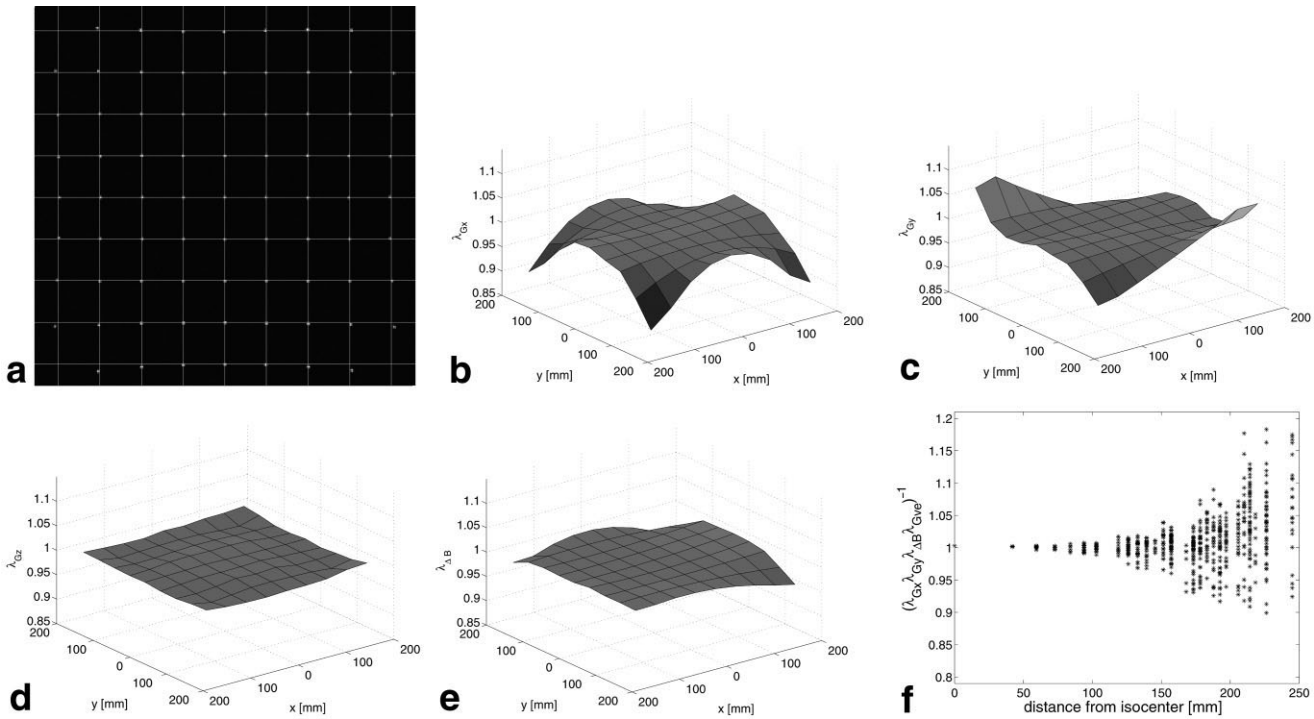

FIG. 4. (**a**) A 2D FT transverse SE image of the phantom through the isocenter with the real grid superimposed on it; (**b–e**) surface renderings of the spatial dependence of the scaling of each gradient coil and the main field in the transverse plane through the isocenter, (**f**) scaling of the flow in the examined volume of 336 × 336 × 336 mm^3 as a function of the off-center distance.

ther off-center clearly exhibit a larger distortion than the tubes close to the isocenter. The corresponding spatial dependence of the specific scaling factors of the 2DPC scans with the flow phantom are rendered in Fig. 4b through e, which demonstrates the symmetrical behavior of the nonlinearity of the gradients. However, this symmetry does not apply around a scaling factor of 1 (no scaling), i.e., in Fig. 4b λ_{Gx} is below 1 at all the corners. The relation between the off-center position of all the grid points within the examined volume and the product of the scaling factors at these points is presented in Fig. 4f, which indicates that flow values will more often be overestimated than underestimated. It also demonstrates that flow scaling increases further off-center and that it increases faster. Errors were well over 10% at off-centers larger than 18 cm and even 20% at 23 cm.

Subsequently, concomitant gradient effects were investigated. Figure 5 clearly shows the effect of concomitant gradients in PC imaging with stationary fluid (Q = 0 mL/sec); the phase offset is of the same sign all over the image and increases quadratically off-center. The mean Q_{mean} and the maximum Q_{max} flow values for different echo times are given in Table 1. The maximum flow values were taken at the largest off-center position. For a TE longer than 20 msec, the mean and maximum value did not decrease significantly any more, indicating that concomitant gradient effects at this echo time were smaller than other error sources. Moreover, at TE = 20 msec, the maximum flow value did not occur at the outer ring of the flow phantom, which is also indicative of other sources of error becoming more important. Therefore, an echo time of 20 msec was chosen. Another reason for this choice was that a longer TE resulted in a lower SNR due to T_2 relaxation (T_2 = 28 msec).

Next, flow measurements were performed with the flow phantom. Timed collection indicated that the flow was 0.78 ± 0.02 mL/sec, which was used as the normalizing

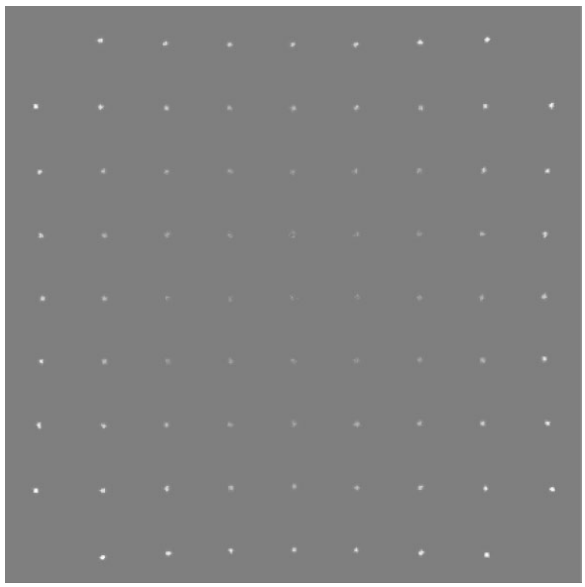

FIG. 5. Thresholded phase image of a transverse 2D PC acquisition through the isocenter with TE = 9.5 msec and stationary fluid (Q = 0 mL/sec). The corresponding mean and maximum flow value are given in Table 1.

Table 1
Mean and Maximum Flow Values (Q_{mean} and Q_{max}) for Different Echo Times and Stationary Fluid (Q = 0 mL/sec) in the Transverse Plane through the Isocenter.

TE (msec)	Q_{mean} (mL/sec)	Q_{max} (mL/sec)
9.5	0.090 ± 0.040	0.20 ± 0.007
12	0.018 ± 0.015	0.061 ± 0.009
16	0.023 ± 0.013	0.057 ± 0.010
20	0.012 ± 0.010	0.025 ± 0.012
24	0.011 ± 0.008	0.024 ± 0.010

The maximum flow value is taken at the largest off-center position. The standard deviation of the mean flow value is calculated from all the flow values in the plane; the standard deviation of the maximum is calculated from the eight measurements of the tube concerned.

value Q_{true}. Normalized 2D PC flow values showed good correlation with the scaling factors determined (r = 0.88) (Fig. 6a). This indicates that correction with the location-specific scaling factors is possible, as is confirmed in Fig. 6b. Correction for concomitant gradient effects increased the correlation coefficient to r = 0.89, which shows that at that line the main bias is caused by scaling due to the nonlinearity of gradients. Nevertheless, it reduces the maximum error even further to less than 5%.

Finally, we proved that correction is also possible in the volunteer study. The lateral positions of the arterial and venous limb of the loop graft model at the forearm of the first volunteer were 227 and 181 mm off-center, respectively. For the second and third volunteer they were the same, namely 220 and 174 mm. The absolute flow values were first corrected for concomitant gradient offsets, measured with stationary fluid. Then, normalization was done with the flow induced by the computer-controlled pump and correction was performed with the local scaling factors. The total local scaling factor was 1.11 for the arterial limb and 1.03 for the venous limb of volunteer 1. For volunteers 2 and 3 they were 1.13 and 0.995. These values indicate that the venous and arterial flow value differ considerably because of their difference in off-center position. Especially at low flow values, the difference is even larger as a result of the same sign of the concomitant gradient offsets for both the venous and the arterial limb, while the flow was of opposite sign as is shown in Fig. 7. In Fig. 7, the results for the venous and arterial limbs of all three volunteers are depicted. They demonstrate that the method of determining local scaling factors worked for both scanners. It can easily be used for correction in combination with correction for concomitant gradient offsets, which makes it independent on flow direction. The normalized arterial flow values of volunteer 1 seem to slightly increase with increasing flow. One explanation may be an underestimation of the concomitant gradient offset in combination with an overestimation of the total local scaling factor. An overestimation of the concomitant gradient bias results in a decreasing trend in the normalized flow value and an underestimation in an increasing trend. Another explanation is the violation of the constant locality conditions as a result of the displacement of the flowing spins.

DISCUSSION

We have shown that inhomogeneity of the main field and nonlinearity of gradients have a significant effect on PC flow measurements; we used a single flow phantom to empirically analyze both phenomena and how they influence the flow values. Information of the spatial dependence of G' and ΔB_0 then allows correction of the observed PC flow values. Moreover, the flow phantom is also well suited to map the 2D PC acquisition-specific concomitant phases.

For 2D PC flow quantification, the nonlinearity of the gradients in all three orthogonal directions plays a role. Namely, the through-plane velocity-encoding nonlinearity causes incorrect velocity encoding of the moving spins and as a result of the in-plane phase and read gradient nonlinearity, geometric distortion of the vessel cross-sectional area occurs. The introduction of the scaling factors made clear that, next to scaling due to inhomogeneity of the main field, the nonlinearity of the gradients is of equal importance, viz. the product of the four independent scal-

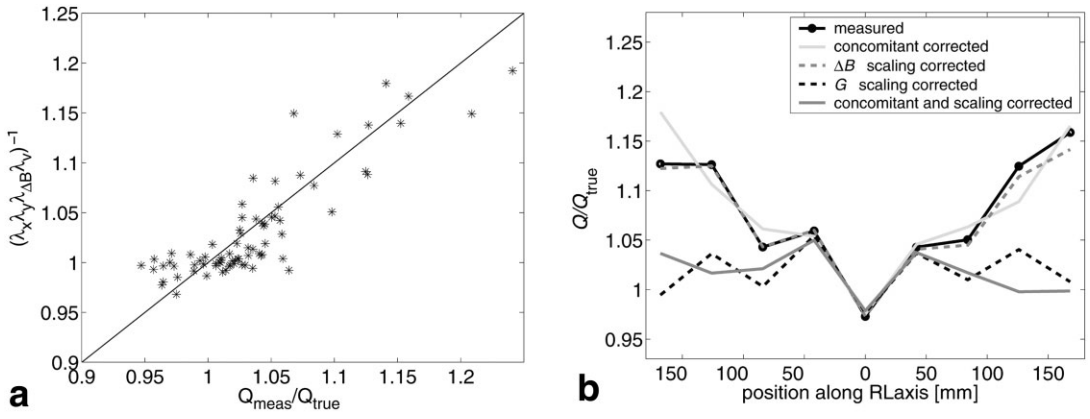

FIG. 6. (**a**) Theoretical and experimental relation between the normalized flow and the scaling factors (asterisks represent the measured points; the solid line shows the theoretical relation of Eq. [7]); (**b**) normalized flow values before and after correction for a line in the transverse plane through the isocenter along the RL-axis 126 mm posterior of the isocenter. The measured values are marked by dots and the lines denote the correction contribution of the different bias causes (scaling due to inhomogeneity of the main field, scaling due to the nonlinearity of gradients, and offsets due to concomitant gradients) and total correction.

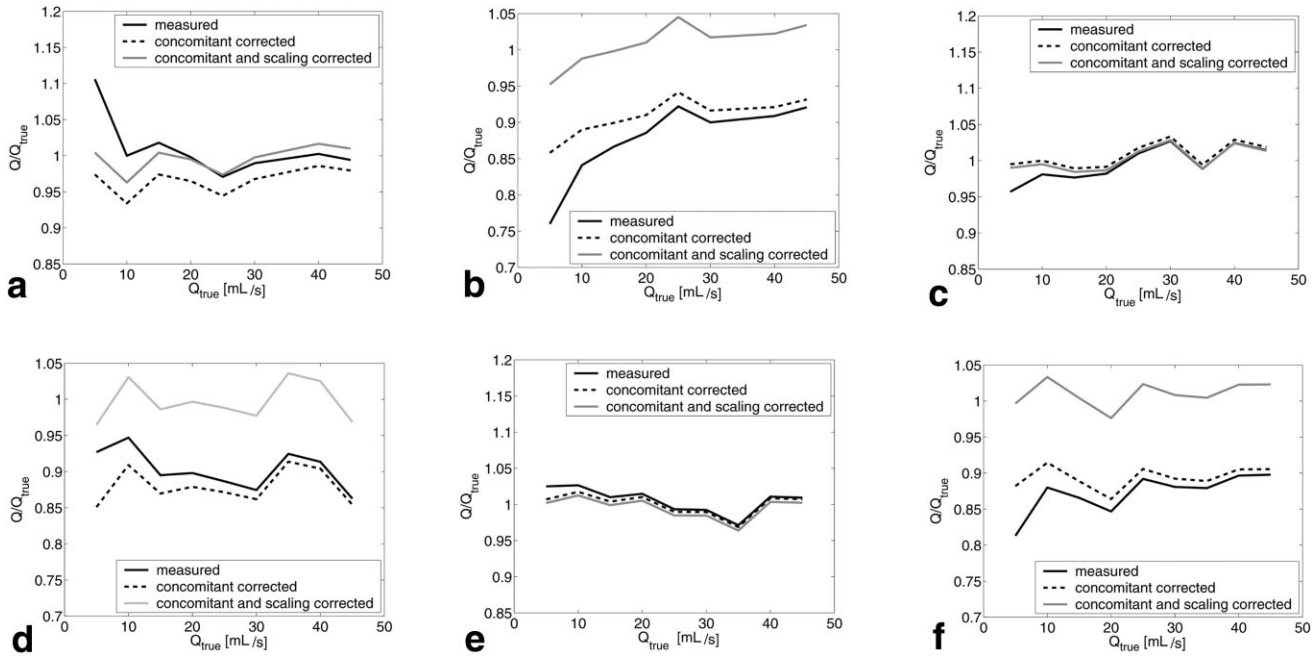

FIG. 7. Normalized measured, concomitant corrected, and concomitant plus scaling corrected flow values of the venous (**a**, **c**, and **e**) and the arterial limb (**b**, **d**, and **f**) of the hemodialysis loop graft phantom at the forearm of the volunteers. The results of volunteer 1 are depicted in the upper row (a, b), those of volunteer 2 in the middle row (c, d), and those of volunteer 3 in the bottom row (e, f).

ing factors determines the biased flow value. The error of the measured flow was as large as 20% at an off-center of 23 cm at system 1. The analysis of the nonlinearity of gradients shows that it causes a geometric distortion that is independent of the gradient strength; the distortion as a result of the inhomogeneity of the main field, however, is dependent on the strength of the read gradient. The influence of ΔB_0 can be diminished by increasing the strength of the read gradient, but at the expense of SNR and, hence, measurement precision. The nonlinearity of the gradients and the inhomogeneity of the main field are machine-dependent, so the actual maps obtained in this study only apply to our machine. The mapping procedure described, however, can be generally applied to any scanner. The results of the loop graft model attached to the forearm of volunteers, who were scanned in two different scanners, confirmed this.

When flow measurements are done at a location where the nonlinearity of gradients and field inhomogeneity are known, correction with the associated scaling factors can be done as long as SNR is sufficient and locality conditions are fulfilled. The correction method is based on scaling factors that are position dependent. If the flow distance of the spins up to the echo time is too long, flow values can no longer be corrected by applying a constant local scaling factor and, instead, the integral over the trajectory of the spins has to be used. This makes the correction more complicated, because the trajectory would have to be known and taken into account in an iterative correction process. This requirement becomes more strict at large off-centers, where the scaling factors depend sensitively on position. Then, in patient examinations, the echo time has to be shortened to fulfill the locality conditions, while in phantom studies, the fluid velocity can be decreased as well. Because of the geometry of the phantom, no object-induced field variations were present. In practice, they can easily be added to the ΔB_0 field and the $\lambda_{\Delta B}$ scaling factor if they are known.

Concomitant gradient phase evolution in phase contrast imaging is dependent on the gradient strengths and the gradient timings. We chose different echo times to investigate the concomitant phase effect, as TE indirectly influences it; a longer echo time allows more freedom in choosing these parameters, and concomitant phase offsets in the phase image can be decreased. However, a longer echo time compromises SNR due to T_2 relaxation. In this case with a circulating fluid with relaxation times of T_1/T_2 = 32/28 msec, it became problematic, but in normal situations with blood ($T_1/T_2 \approx 1200/200$ msec) long echo times can be used as long as displacements are not too large. We used the remaining concomitant gradient phase of the stationary fluid at TE = 20 msec for correction of the flow measurements, which also resulted, in combination with scaling correction, in a better measurement accuracy.

A potentially relevant application of PC flow measurements is the loop graft of hemodialysis patients. Poor flow rates reduce dialysis efficiency and are indicative of impending graft thrombosis due to higher flow resistance (18). At flow values below 10 mL/sec, in most cases stenotic area(s) exists within the loop graft (19,20). The measurements in the loop graft model attached to the forearm of volunteers showed that flow measurements at eccentric positions are degraded by the nonlinearity of gradients, inhomogeneity of the main field, and concomitant gradient phase evolution. They demonstrated a difference between the 2D PC flow values of the arterial and venous limb of the loop graft. When clinical decisions, e.g., intervention to decrease the resistance at flow values below the threshold

of 10 mL/sec, depend on these measurements, biased flow values can give incorrect indications. Therefore, the best position of the forearm is close to the isocenter, as scaling and concomitant gradient errors exist at eccentric locations. However, when the patient cannot be in that position for the required scan time, which often is the case for hemodialysis patients, measurements have to be done at an off-center location and flow values will be biased. Our correction method allows us to compensate for this bias and shows a significant improvement in measurement accuracy. Especially at low flow values with low velocity contents, the sequence-dependent concomitant gradient offsets have to be prevented by long echo times or have to be compensated by measuring the spatial offsets or analytical analysis (16). The correction method may also be practical in other applications, like open magnet scanners, in which field inhomogeneity is generally larger than in conventional scanners. However, positioning of the patient in open magnet scanners is less restricted by the scanner setup and the forearm can be positioned at the isocenter more easily.

ACKNOWLEDGMENT

The authors thank Dr. M. A. Moerland for kindly providing the flow phantom.

REFERENCES

1. Andersen AH, Kirsch JE. Analysis of noise in phase contrast MR imaging. Med Phys 1996;23:857–869.
2. Bakker CJG, Hoogeveen RM, Viergever MA. Construction of a protocol for measuring blood flow by two-dimensional phase-contrast MRA. J Magn Reson Imaging 1999;9:119–127.
3. Bakker CJG, Kouwenhoven M, Hartkamp MJ, Hoogeveen RM, Mali WPTM. Accuracy and precision of time-averaged flow as measured by nontriggered 2D phase-contrast MR angiography, a phantom evaluation. Magn Reson Imaging 1995;13:959–965.
4. Buonocore MH, Bogren H. Factors influencing the accuracy and precision of velocity-encoded phase imaging. Magn Reson Med 1992;26: 141–154.
5. Greil G, Geva T, Maier SE, Powell AJ. Effect of acquisition parameters on the accuracy of velocity encoded cine magnetic resonance imaging blood flow measurements. J Magn Reson Imaging 2002;15:47–54.
6. Robertson MB, Köhler U, Hoskins PR, Marshall I. Quantitative analysis of PC MRI velocity maps: pulsatile flow in cylindrical vessels. Magn Reson Imaging 2001;19:685–695.
7. Tang C, Blatter DD, Parker DL. Accuracy of phase-contrast flow measurements in the presence of partial-volume effects. J Magn Reson Imaging 1993;3:377–385.
8. Wolf RL, Ehman RL, Riederer SJ, Rossman PJ. Analysis of systematic and random error in MR volumetric flow measurements. Magn Reson Med 1993;30:82–91.
9. Markl M, Bammer R, Alley MT, Elkins CJ, Draney MT, Barnett A, Mosely ME, Glover GH, Pelc NJ. Generalized reconstruction of phase contrast MRI: analysis and correction of the effect of gradient field distortions. Magn Reson Med 2003;50:791–801.
10. Bosman PJ, Boereboom FTJ, Bakker CJG, Mali WPTM, Eikelboom BC, Blankestijn PJ, Koomans HA. Access flow measurements in hemodialysis patients: in vivo validation of an ultrasound dilution technique. J Am Soc Nephrol 1996;7:966–969.
11. Reichenbach JR, Venkatesan R, Yablonski DA, Thompson MR, Lai S, Haacke EM. Theory and application of static field inhomogeneity effects in gradient-echo imaging. J Magn Reson Imaging 1997;7:266–279.
12. Drangova M, Pelc NJ. Artifacts and signal loss due to flow in the presence of B_0 inhomogeneity. Magn Reson Med 1996;35:126–130.
13. Moerland MA. Magnetic resonance imaging in radiotherapy treatment planning. Ph.D. thesis, Utrecht University, 1996.
14. Schenck JF. The role of magnetic susceptibility in magnetic resonance imaging: MRI magnetic compatibility of the first and second kinds. Med Phys 1996;23:815–850.
15. Bakker CJG, Moerland MA, Bhagwandien R, Beersma R. Analysis of machine-dependent and object-induced geometric distortion in 2DFT MR imaging. Magn Reson Imaging 1992;10:597–608.
16. Bernstein MA, Joe Zhou X, Polzin JA, King KF, Ganin A, Pelc NJ, Glover GH. Concomitant gradient terms in phase contrast MR: analysis and correction. Magn Reson Med 1998;39:300–308.
17. Smits HFM, Bos C, Van der Weide R, Bakker CJG. Endovascular interventional MR: balloon angioplasty in a hemodialysis access flow phantom. J Vasc Interv Radiol 1998;9:840–845.
18. Bosman PJ, Boereboom FTJ, Eikelboom BC, Koomans HA, Blankestijn PJ. Graft flow as a predictor of thrombosis in hemodialysis grafts. Kidney Int 1998;54:1726–1730.
19. Bosman PJ, Boereboom FTJ, Smits HFM, Eikelboom BC, Koomans HA, Blankestijn PJ. Pressure or flow recordings for the surveillance of hemodialysis grafts? Kidney Int 1997;52:1084–1088.
20. Blankestijn PJ, Smits JHM. How to identify the haemodialysis access at risk of thrombosis? Are flow measurements the answer? Nephrol Dial Transplant 1999;14:1068–1071.